JOURNAL OF AIRCRAFT
Vol. 46, No. 1, January–February 2009

Engineering Notes

ENGINEERING NOTES are short manuscripts describing new developments or important results of a preliminary nature. These Notes should not exceed 2500 words (where a figure or table counts as 200 words). Following informal review by the Editors, they may be published within a few months of the date of receipt. Style requirements are the same as for regular contributions (see inside back cover).

Effect of Taper Ratio on Aerodynamic Performance of Cropped Nonslender Delta Wings

P. F. Zhang,* J. J. Wang,† Y. Liu,‡ and Z. Wu§
Beijing University of Aeronautics and Astronautics, 100083 Beijing, People's Republic of China

DOI: 10.2514/1.32130

I. Introduction

THE slender delta wing ($\Lambda \geq 65$ deg) has many advantages in highly maneuverable fighter aircraft and supersonic civil transport. The flow over slender delta wings has been extensively studied and is now reasonably well understood [1–3]. Recently, the nonslender delta wings or low-sweep delta wings ($\Lambda \geq 55$ deg) have been used in a variety of unmanned air vehicles and micro air vehicles (MAV), and the flow over low-sweep delta wings has attracted increasing attention [4–7]. Compared with the slender delta wings, the flow structures and the aerodynamic characteristics of low-sweep delta wings exhibit distinct differences, but less research has been undertaken for these nonslender delta wing configurations.

It is well known that the flow over a slender delta wing at high angles of attack is dominated by two large counter-rotating leading-edge vortices that are formed by the roll-up of vortex sheets. The development of the leading-edge vortex will generate large axial and swirl velocity components and will result in low pressure in the vortex core, which generates additional suction and lift force on the delta wings. Compared with the slender delta wing, the vortices generated over low-sweep planforms are formed much closer to the wing surface [4]. The interaction between the leading-edge vortices and the boundary layer is a typical characteristic of the flow around the nonslender delta wing, particularly at low angles of attack. This results in the structure of vortical flows being highly dependent on the Reynolds number. The dye flow visualization experiment of Gursul et al. [5] presented the vortices generated over the wing at an incidence of $\alpha = 5$ deg for three different Reynolds numbers. The leading-edge vortex breakdown is visible for $Re = 8700$. As the Reynolds number increases to 13,000, the breakdown of the vortex progresses upstream, which is a curious result considering the accepted insensitivity of vortices and vortex breakdown over slender delta wings. When the Reynolds number is increased to $Re = 26,000$, the vortex breakdown location moves to nearly 40% of the chord length. Another unique feature of the low-sweep wings is the formation of a dual-vortex structure [5,6]. The dual-vortex structure is two vortices formed at the same leading edge of the delta wing, and they rotate in the same direction. Gordnier and Visbal [6] indicated that the dual-vortex structure is formed due to secondary separation splitting the primary vortex into two separate concentrations of vorticity. This feature is more commonly observed at lower incidences when the vortices are formed closest to the wing surface, and it is highly sensitive to Reynolds number. A single layer of vorticity concentration was observed at very low Reynolds numbers and the dual-vortex structure was absent. With the increase of Reynolds number, the significant interaction between the boundary layer and primary vortex results in this dual-vortex structure [5].

One of the aerodynamic problems on MAVs is the effect of low aspect ratio, which is induced by the restriction of size of the MAV. To achieve a large wing area with a limited wing span, the chord length is almost the same as the span and the aspect ratio is usually smaller than 2. According to the past investigations on low-aspect-ratio wings at high Reynolds numbers, the tip vortices were observed to affect a large portion of the upper wing surface. The low pressure caused by the vortices increases both the lift and drag forces. In general, the tip vortex effects are twofold:

1) The tip vortex causes downwash, which decreases the effective angle of attack and increases the drag force.

2) The tip vortex forms a low-pressure region on the upper surface of the wing, which provides additional lift force [8].

Lian and Shyy [9] studied the tip vortex effect on the aerodynamic performance of the micro air vehicle. They found that the vortical flow is usually associated with a low-pressure zone. The pressure drop further strengthens the swirl by attracting more fluids toward the vortex core; meanwhile, the pressure decreases correspondingly in the vortex core. The low-pressure region created by the vortex generates additional lift. Toward downstream, the pressure recovers to its ambient value, the swirling weakens, the diameter of the vortex core increases, and the vortex core losses its coherent structure. But the tip vortex induces downwash movement that reduces the effective angle of attack. When a wing has a relatively low aspect ratio, such as that employed by the MAV, the induced drag by the tip vortex is relatively large and therefore the aerodynamic performance of the vehicle is deteriorated. Viieru et al. [10] investigated the effect of the end plate on wing aerodynamic performances as a method to assess the induced drag. The investigation is facilitated by solving the Navier–Stokes equations around a rigid wing with a root chord Reynolds number of 9×10^4. They confirmed that the end plate paralleling with the freestream velocity increases lift without a significant decrease in induced drag. The end plate reduces the flow going from the lower surface to the upper surface of the wing, effectively reducing the downwash and increasing the effective angle of attack. However, the effectiveness of the end plate diminishes as the angle of attack increases, due to a stronger wing tip vortex.

More recently, Pelletier and Mueller [11] investigated the low Reynolds number aerodynamics of a variety of cambered and uncambered wings with low aspect ratios. Their study included experiments with semispan models of semi aspect ratios varying from 0.5 to 3.0 at Reynolds numbers less than 200,000. The results show that the lift-curve slope reduces with decreasing aspect ratio. Furthermore, as the aspect ratio is decreased, the linear region of the lift-coefficient-vs-α curve becomes longer and the stall angle

Received 14 May 2007; revision received 3 June 2008; accepted for publication 3 June 2008.

*Associate Professor, Institute of Fluid Mechanics; pfzhang@buaa.edu.cn.
†Professor, Institute of Fluid Mechanics; jjwang@buaa.edu.cn.
‡Graduate Student, Institute of Fluid Mechanics; antony@ase.buaa.edu.cn.
§Professor, Department of Flight Design; wuzhe@buaa.edu.cn.

increases. Changing the aspect ratio of the models does not appear to have a strong effect on the drag coefficient at $Re = 8 \times 10^4$. At $Re = 1.4 \times 10^5$, increasing the aspect ratio has the unexpected effect of increasing the drag coefficient for angles greater than 5 deg. But the low-aspect-ratio wing model used in their experiments is attached with two aluminum end plates, which will interact with the wing model and affect the aerodynamic force of the wing.

In practical MAV designs, the delta wing planform is more like a cropped nonslender delta wing with a low-sweep leading edge. But little work has been done to examine aerodynamic characteristics of this wing planform. The main objective of this work is to study the effect of taper ratio on the aerodynamics of the cropped nonslender delta wings with a 40 deg swept leading edge. The lift and drag were measured in the wind tunnel and the topological flow structure on the suction surface of the delta wing was presented by oil flow visualization. The leading-edge-suction analogy can also predict the lift and drag coefficients of the cropped delta wings with the taper ratio from 0 to 0.79.

II. Experiment Setup

The experiment is conducted in the D1 open-circuit low-speed wind tunnel of Beijing University of Aeronautics and Astronautics. The test section of the tunnel is nominally 0.76 m high, 1.02 m wide, with a quasi-elliptical cross section, and 1.5 m long. The turbulence intensity of the freestream velocity is about 1%, and the mean deflection of the incoming flow is less than 0.1 deg. There are 16 cropped nonslender delta wing models with a 40 deg swept leading edge used in the present study, which have a root chord length $c_r = 200$ mm. The taper ratio of the models $\lambda = c_t/c_r$ varies from 0 to 0.79, where c_t is the tip chord length of the delta wing. The aspect ratio based on the root chord has a range of $AR1 = b/c_r = 0.5$–2.38 and the corresponding aspect ratio based on the mean aerodynamic chord $AR2 = b^2/s$ changes from 0.56 to 4.77 (b and s are the span length and area of the delta wing, respectively). The detail parameters of the taper ratio and the aspect ratio are presented in Table 1. All the models are made of an aluminum plate with a thickness of 3 mm and are beveled 45 deg at the upside leading edge of the delta wings. The sketch of the model and the geometry parameters can be seen in Fig. 1.

The time-averaged lift and drag forces of the delta wing are measured by a six-component internal strain gauge balance. The forces and moments are normalized to give coefficients of lift and drag $C_L = L/0.5\rho U_\infty^2 s$ and $C_D = D/0.5\rho U_\infty^2 s$, where L and D are the lift and drag, respectively; s is the reference area; and ρ is the fluid density. The deviation of the lift and drag coefficients is less than 3%. On-body flow visualization is achieved by oil flow tests. A mixture of oil (kerosene) and titanium dioxide powder was applied to the upper surface of the delta wing. The tunnel is rapidly brought to test speed, and shear lines form in the mixture as air flows over the model. Photographs of the established flow patterns are then obtained from multiple angles using a digital camera. The model in the wind tunnel is supported at the middle part of the trailing edge. The angle-of-attack ranges have two values because the lift curves of the delta wing with different taper ratios have two totally different stall features. With taper ratio $\lambda = 0$–0.3, the angles of attack vary from -4 to 40 deg, but with taper ratio $\lambda = 0.3$–0.79, the angle-of-attack range is -4 to 60 deg. The angle step for all cases is 2 deg. The freestream velocities in force measurement and oil flow test have the same value $U_\infty = 20$ m/s, and the Reynolds number based on the root chord length of the delta wing is $Re = 3.42 \times 10^5$. The results in this Note are the original experimental data without any correction.

Table 1 Taper ratios and the corresponding aspect ratios of the delta wings

$\lambda = c_t/c_r$	0	0.02	0.04	0.06	0.08	0.1	0.2	0.3
$AR1 = b/c_r$	2.38	2.34	2.29	2.24	2.19	2.15	1.91	1.67
$AR2 = b^2/s$	4.77	4.58	4.40	4.23	4.06	3.90	3.18	2.57
$\lambda = c_t/c_r$	0.4	0.45	0.5	0.58	0.625	0.685	0.725	0.79
$AR1 = b/c_r$	1.43	1.31	1.19	1	0.89	0.75	0.66	0.5
$AR2 = b^2/s$	2.04-	1.81	1.59	1.27	1.10	0.89	0.76	0.56

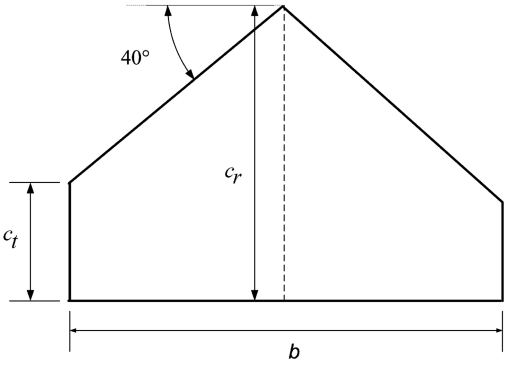

Fig. 1 Sketch of the 40 deg delta wings and the geometry parameters.

III. Lift and Drag Characteristics

The variation of C_L against α with different taper ratios is shown in Fig. 2. The lift coefficients at zero angle of attack in all cases are less than 0 due to the single-side-beveled leading edge and the deviation in model mounting, which means that the model cannot be fixed symmetrically about the horizontal plane. Because the study just investigates the effect of taper ratio on the aerodynamic performance of the delta wing, the deviation of lift coefficients at zero angle of attack is taken as a system error without correction. When the taper ratio λ is less than 0.3 (in Fig. 2a), all the lift curves nearly collapse to the same one, which indicates that the taper ratio has no influence on the lift coefficient of the delta wing in this regime. When the taper ratio is larger than 0.3 (in Fig. 2b), the lift characteristics of the delta wings have much difference. The lift-curve slope C_L/α increases with the increase of taper ratio in the region $-4\,\text{deg} \le \alpha \le 10\,\text{deg}$, then it has the same value independent of λ until the stall angle of attack. The second obvious difference of the lift curves is the stall behavior: with $0.3 \le \lambda \le 0.5$, the lift drops slowly after the stall point. After that ($\lambda \ge 0.58$), the lift curve begins to drop quickly and has a sudden drop with $\lambda = 0.625$, which is the so-called abrupt stall. Then, when the taper ratio increases to 0.68, the lift curve presents a slow stall behavior again. With regard to the two largest values of taper ratio in the present study ($\lambda = 0.725$ and 0.79), the lift curve has a region of abrupt enhancement behind the stall point.

Corresponding to the lift characteristics, Fig. 3 presents the oil flow visualization photos on the upper surface of the delta wings with taper ratios $\lambda = 0$, 0.3, and 0.5. It is obvious that the flow around the delta wing with $\lambda = 0$ has four typical stages with the angle-of-attack variation for the noncropped delta wing.

The first stage is the leading-edge separation bubble at low angles of attack (see the first image in Fig. 3a at $\alpha = 5$ deg), but the separation bubble is three-dimensional and has spiral flow, which is different from the two-dimensional case in the flow around the airfoil.

The second stage is the concentrated leading-edge vortex ($\alpha = 10$, 15, and 20 deg in Fig. 3a), which can be seen from the reattached line of the separated shear layer on the delta wing suction surface. Although the leading-edge vortex is not clearly visible for the nonslender delta wing ($\Lambda = 40$, 50, and 55 deg) by the schlieren system in the wind tunnel [12], the dye inject visualization [5,13] and the particle image velocimetry method [5] can present this concentrated vortex of nonslender delta wings. This is because the leading-edge vortex of the nonslender delta wing is much weaker than that of the slender delta wing, and the pressure gradient and density variation induced by the leading-edge vortex is small, which results in the failure to visualize the leading-edge vortex by the schlieren method.

The third stage is that spiral flow appears on the suction side of the delta wing at $\alpha = 25$ deg (in Fig. 3a), which is larger than the angle corresponding to the vortex breakdown on the apex of the delta wing.

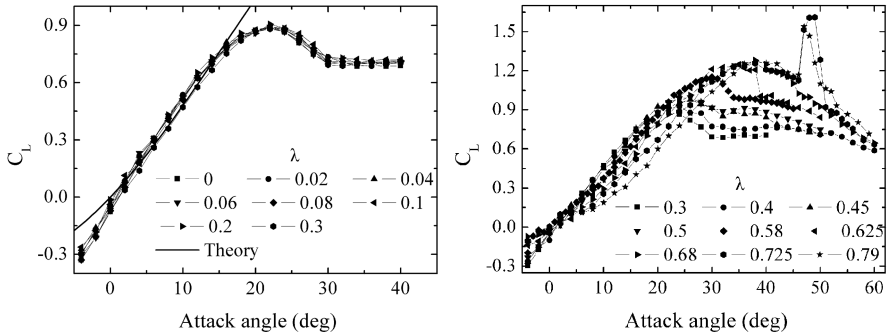

a) λ = 0~0.3 **b) λ = 0.3~0.79**

Fig. 2 Lift coefficient as a function of angle of attack with different taper ratios.

This value matches well with the stall angle obtained by force measurement of a 40 deg swept delta wing ($\alpha = 22$ deg). The feature for this spiral flow is the spiral point in the oil flow pattern on the suction surface of the delta wing.

In the fourth stage ($\alpha = 30$ deg in Fig. 3a) there is a big region of adverse flow on the upper surface of the delta wing, and the lift of the delta wing becomes much smaller. The difference between the oil flow patterns of the noncropped and cropped delta wings is the spiral

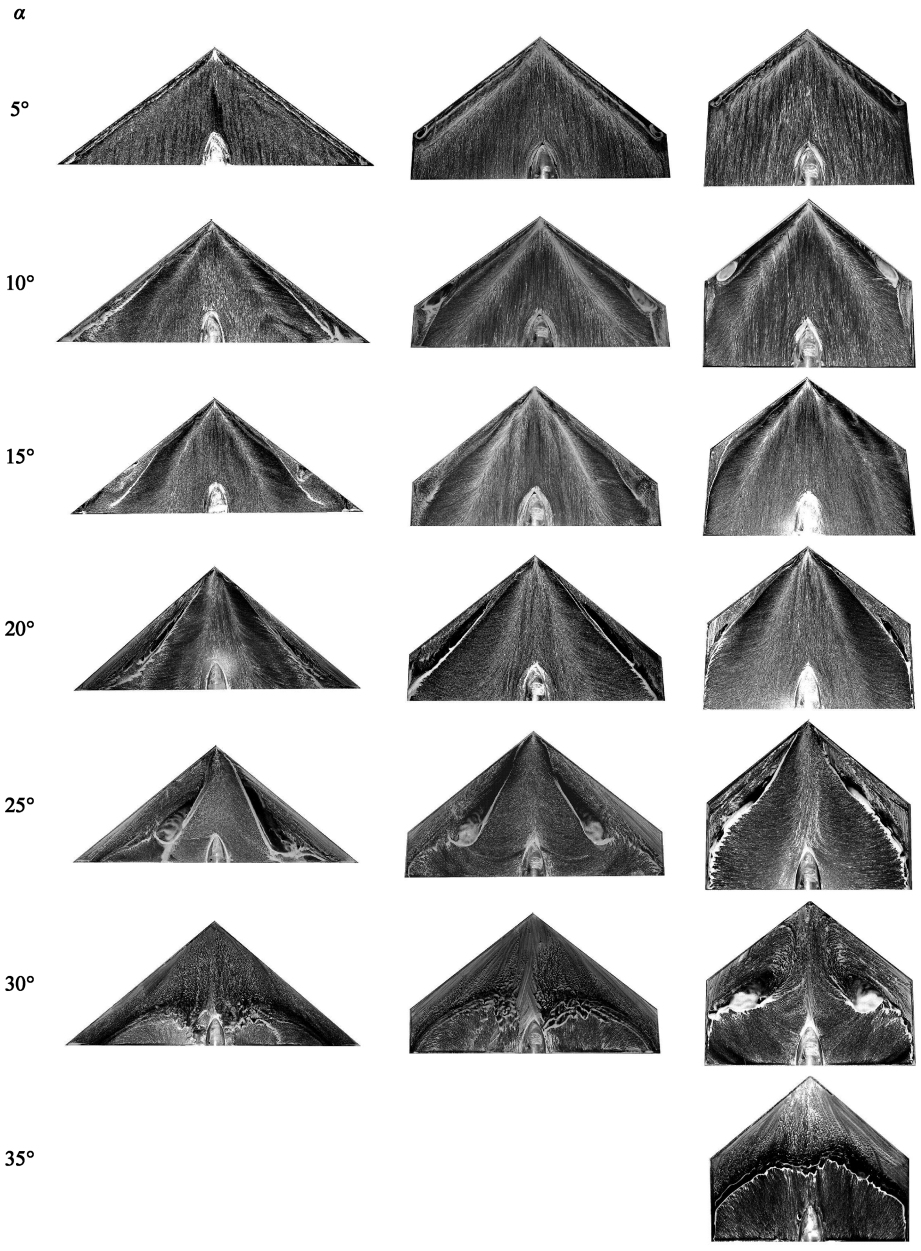

a) λ = 0 **b) λ = 0.3** **c) λ = 0.5**

Fig. 3 Oil flow visualization on the upper surface of the delta wings.

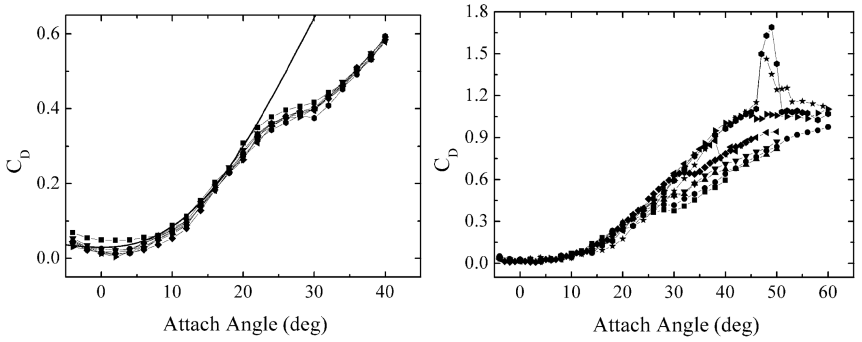

a) λ = 0~0.3 **b) λ = 0.3~0.79**

Fig. 4 Drag coefficient as a function of angle of attack with different taper ratios.

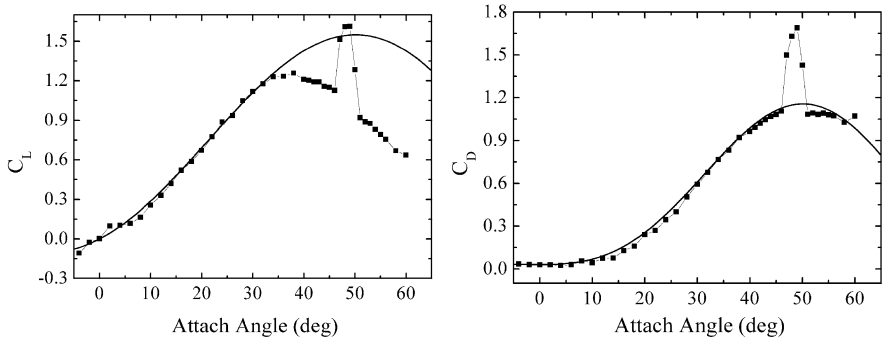

a) Lift **b) Drag**

Fig. 5 Experimental data and the fitting curves by leading-edge-suction analogy with $\lambda = 0.725$.

point in the kink region of the leading edge before stall (shown in the second image of Figs. 3b and 3c at $\alpha = 10$ deg). At this angle of attack, the leading-edge vortex begins to form, but not strong enough to eliminate the disturbance of the tip vortex, and the interaction between them makes the spiral-point appearance.

The oil flow visualization in the present study is just a simple way to capture the time-averaged near-wall flow direction features, and so it cannot present the complex and unsteady flow structures. The aerodynamic characteristics of the cropped delta wing with large taper ratio (such as the increase of the maximum lift with taper ratio, the stall features, and the abrupt lift-enhancement region after stall with $\lambda = 0.725$ and 0.79) are associated with the interaction of the leading-edge vortex of the delta wing and the tip vortex. The flow structure is complex and unsteady, and so the oil flow visualization cannot explain the mechanism of these phenomena. As a note, the present study just indicated these unusual aerodynamic characteristics of the cropped delta wing, and it needs further investigation through particle image velocimetry, laser Doppler velocimetry, or hot-wire measurements, which can obtain the detailed flowfield information and the instant variation of the flow parameters.

Figure 4 presents the drag coefficient vs the angle of attack with different taper ratios. Similar to the lift curves, the drag-characteristic variation with the taper ratio has two different regimes. For the taper ratio $0 < \lambda \leq 0.3$ (shown in Fig. 4a), the taper ratio has no effect on the drag of cropped delta wings, but the drags of all cropped delta wings are less than the base case (the 40 deg swept delta wing $\lambda = 0$) for the angles of attack less than 10 deg. It can be concluded that the maximum lift-to-drag ratio can be enhanced for the cropped delta wings, because the angle of attack corresponding to the maximum lift-to-drag ratio belongs to the region $\alpha < 10$ deg for the delta wings investigated in the present study. Meanwhile, the drags of the cropped delta wings are reduced in the range of $\alpha = 20$–30 deg after stall. For the taper ratio $\lambda = 0.3$–0.79 (shown in Fig. 4b), the drags of delta wings do not vary with the taper ratio at low angles of attack ($\alpha < 10$ deg). In the region after stall angle ($\alpha > 20$ deg), the drag of the delta wing increases with the taper ratio, because the lift-induced drag increases corresponding to the lift enhancement in Fig. 2b. It is obvious that the drag variation is dependent on the lift for the cropped delta wing, such as with the abrupt drop of drag for $\lambda = 0.68$ and the sudden spikes of drag curves for $\lambda = 0.725$ and 0.79.

IV. Leading-Edge-Suction Analogy

It is common in prediction methods based on the leading-edge-suction analogy to decompose lift into two components. One is due to attached or potential flow and the other comprises the nonlinear vortex lift. In the leading-edge-suction analogy, the vortex lift is assumed to be equal to the leading-edge suction that would have been developed in the absence of leading-edge separation. Polhamus [14] decomposed the lift coefficient as follows:

$$C_L = K_p \sin\alpha\cos^2\alpha + K_v \cos\alpha\sin^2\alpha \tag{1}$$

where K_p is the potential lift factor and K_v is the vortex lift factor. The vortex lift factor is usually not affected by the aspect ratio and the geometric parameters of the delta wing and falls within a 10% band around π [15]. In the present study, all the fitting curves are plotted with $K_v = \pi$. The line without a symbol in Fig. 2a is fitted by the formula (1) with $K_p = 2.3$. The theory fitting curve totally matches the experimental data before the leading-edge vortex breakdowns, which corresponds to the angle of attack before stall. The divergence between them at negative angles of attack is caused by the single-side-beveled leading edge and the deviation in model mounting mentioned in Sec. III. For the cases with large taper ratio values ($\lambda = 0.3$–0.79), the linear parts of the lift curves are varied with different taper ratios and the lift is not in a linear relationship with angle of attack at onset, but the theory curve fits well with the experimental data by adjusting the potential lift factor K_p. Figure 5a presents the experimental lift data for $\lambda = 0.725$ and the theory fitting curve. They totally collapse to the same one in the range $\alpha = -4$–30 **deg** before stall. These results indicate that the leading-edge-suction analogy can be used to predict the cropped nonslender delta wing investigated in this Note.

To determine the drag of the delta wing, Phillips and Snyder [16] modified Prandtl's classic lifting line theory and gave a theory formula as follows:

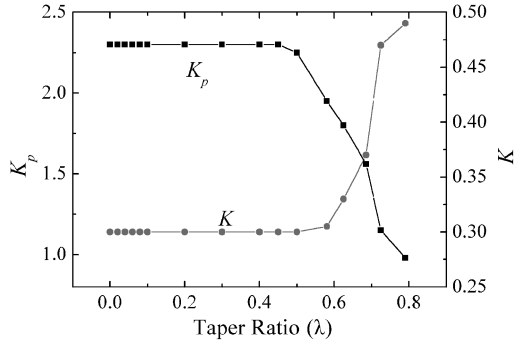

Fig. 6 Variation of the potential lift factor and the lift-induced drag factor with taper ratio.

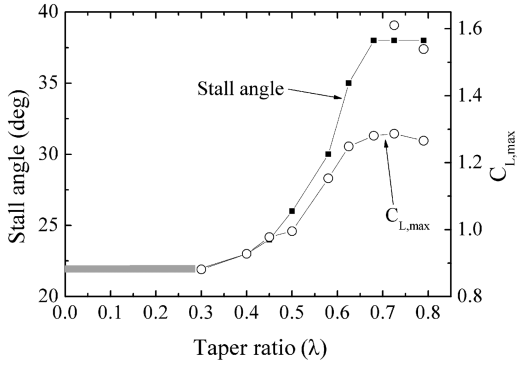

Fig. 7 Effect of taper ratio on the stall angle and maximum lift coefficient of the delta wing.

$$C_D = C_{D0} + K(C_L)^2 \tag{2}$$

where C_{D0} is the zero-lift drag, and $K(C_L)^2$ is the lift-induced drag (K is the lift-induced drag factor). For the delta wings in the present study, the zero-lift drags have the same value $C_{D0} = 0.03$ as that obtained by fitting. Figures 4a and 5b present the experimental drag data and the theory fitting curves, and they also match well, as with the preceding lift. In the curve fitting with theory formulas (1) and (2), the vortex lift factor K_v and the zero-lift drag C_{D0} have constant values, then the effect of taper ratio on the lift and drag characteristics is presented by the variation of the potential lift factor K_p and the lift-induced drag factor K. Figure 6 shows that these two factors vary with the taper ratio. When the taper ratio is less than 0.5, the potential lift factor and the induced-drag factor have constant values ($K_p = 2.3$ and $K = 0.3$), because the tip vortex formed over the delta wing is not strong enough to affect the aerodynamic of the delta wing. When λ is larger than 0.5, K_p decreases quickly with the taper ratio increase, because the downwash effect on the incoming flow induced by the tip vortex increases with the taper ratio. On the other hand, the lift-induced drag factor K increases with taper ratio, which means that the lift-induced drag increases with taper ratio. This conclusion is consistent with that in Sec. III. With the taper ratio increase, the tip vortex formed on the cropped delta wing will be enhanced, and so the lift-induced drag will certainly increase.

V. Conclusions

The force measurement and oil flow visualization experiments are carried out in a wind tunnel to investigate the aerodynamic performance of the cropped nonslender delta wings with 40 deg swept leading edge. The effect of taper ratio ($\lambda = 0$–0.79) on the lift and drag of the delta wing is studied.

When the taper ratio is in the range of $\lambda = 0$–0.3, the drag of all cropped delta wings at low angles of attack is less than that of the noncropped wing, and so the lift-to-drag ratio of the cropped delta wing in this region would be enhanced. With the taper ratio of $\lambda = 0.3$–0.79, the stall angle of the delta wing will be delayed with the taper ratio, and the maximum lift coefficient also increases. Figure 7 summarizes the effect of taper ratio on the stall angle and maximum lift coefficient of the delta wing, in which the maximum lift coefficient has two values for $\lambda = 0.68$–0.79. One corresponds to the maximum lift coefficient during slow stall, and the other presents the maximum lift coefficient in the lift-enhancement region after the stall point. It is obvious that the stall angle and the maximum lift have constant values for the taper ratio $\lambda < 0.3$. Because as the taper ratio is in the range of $\lambda = 0.3$–0.68, the two parameters increase with the taper ratio, and they reach the maximum values with $\lambda = 0.725$ and 0.79. The stall angle of the delta wing with $\lambda = 0.725$ and 0.79 is delayed from 22 to 38 deg compared with that of the noncropped delta wing, and the maximum lift coefficient is enhanced from 0.88 to 1.27, even reaching 1.55 in the lift-enhancement region after stall for $\lambda = 0.725$ and 0.79.

The leading-edge vortex-suction analogy can also predict the lift and drag coefficients of the cropped delta wings in the present study. When the taper ratio is less than 0.5, the potential lift factor and the induced-drag factor have constant values ($K_p = 2.3$ and $K = 0.3$). When λ is larger than 0.5, K_p decreases quickly with the taper ratio increase, which indicates that the potential lift deceases with taper ratio increase. But the lift-induced drag factor K increases with taper ratio increase.

Acknowledgments

The present research was supported by the National Natural Science Foundation of China under grant NSFC-10425207 and the China Aviation Science and Technology Creation Funding under grant 07A51001.

References

[1] Gursul, I., "Review of Unsteady Vortex Flows over Slender Delta Wings," *Journal of Aircraft*, Vol. 42, No. 2, 2005, pp. 299–319. doi:10.2514/1.5269

[2] Lin, J. C., and Rockwell, D., "Transient Structure of Vortex Breakdown on a Delta Wing," *AIAA Journal*, Vol. 33, No. 1, 1995, pp. 6–12. doi:10.2514/3.12325

[3] Delery, J. M., "Aspects of Vortex Breakdown," *Progress in Aerospace Sciences*, Vol. 30, No. 1, 1994, pp. 1–59. doi:10.1016/0376-0421(94)90002-7

[4] Gursul, I., "Recent Developments in Delta Wing Aerodynamics," *The Aeronautical Journal*, Vol. 108, No. 1087, 2004, pp. 437–452.

[5] Gursul, I., Gordnier, R., and Visbal, M., "Unsteady Aerodynamics of Nonslender Delta Wings," *Progress in Aerospace Sciences*, Vol. 41, No. 7, 2005, pp. 515–557. doi:10.1016/j.paerosci.2005.09.002

[6] Gordnier, R. E., and Visbal, M. R., "Compact Difference Scheme Applied to Simulation of Low-Sweep Delta Wing Flow," *AIAA Journal*, Vol. 43, No. 8, 2005, pp. 1744–1752. doi:10.2514/1.5403

[7] Wang, J. J., and Lu, S. F., "Effects of Leading-Edge Bevel Angle on the Aerodynamic Forces of a Nonslender 50 Degrees," *The Aeronautical Journal*, Vol. 109, No. 1098, 2005, pp. 403–407.

[8] Lian, Y., Shyy, W., Viieru, D., and Zhang, B., "Membrane Wing Aerodynamics for Micro Air Vehicles," *Progress in Aerospace Sciences*, Vol. 39, Nos. 6–7, 2003, pp. 425–465. doi:10.1016/S0376-0421(03)00076-9

[9] Lian, Y., and Shyy, W., "Three-Dimensional Fluid-Structure Interactions of a Membrane Wing for Micro Air Vehicle Applications," *Journal of Aircraft*, Vol. 42, No. 4, 2005, pp. 865–873. doi:10.2514/1.5909

[10] Viieru, D., Lian, Y., and Shyy, W., "Investigation of Tip Vortex on Aerodynamic Performance of a Micro Air Vehicle," AIAA Paper 2003-3597, 2003.

[11] Pelletier, A., and Mueller, T. J., "Low Reynolds Number Aerodynamics of Low-Aspect-Ratio, Thin/Flat/Cambered Plate Wings," *Journal of Aircraft*, Vol. 37, No. 5, 2000, pp. 825–832.

[12] William, H., Wentz, J., and David, L. K., "Wind Tunnel Investigations of Vortex Breakdown on Slender Sharp-Edged Wings," NASA Rept. N69-14762, 1968.

[13] Chakrabartty, S. K., Dhanalakshmi, K., and Mathur, J. S., "Navier-Stokes Analysis of Vortex Flow over a Cropped Delta Wing," *Acta*

Mechanica, Vol. 131, Nos. 1–2, 1998, pp. 69–87.
doi:10.1007/BF01178245

[14] Polhamus, E. C., "A Concept of the Vortex Lift of Sharp-Edge Delta Wings Based on a Leading-Edge-Suction Analogy," NASA TN D-3767, 1966.

[15] Lamar, J. E., "Extension of Leading-Edge Suction Analogy to Wings with Separated Flow Around the Side Edges at Subsonic Speeds," NASA TR R-428, 1974.

[16] Phillips, W. F., and Snyder, D. O., "Modern Adaptation of Prandtl's Classic Lifting-Line Theory," *Journal of Aircraft*, Vol. 37, No. 4, 2000, pp. 662–670.